

**Porous protein crystals as scaffolds for enzyme immobilization**

Journal:	<i>Biomaterials Science</i>
Manuscript ID	BM-ART-10-2018-001378.R1
Article Type:	Paper
Date Submitted by the Author:	05-Jan-2019
Complete List of Authors:	Kowalski, Ann; Colorado State University, Chemical and Biological Engineering Johnson, Lucas; Colorado State University, Chemical and Biological Engineering Dierl, Holland; Colorado State University, Chemical and Biological Engineering Park, Seho; Colorado State University, Chemical and Biological Engineering Huber, Thaddaus; Colorado State University, Chemical and Biological Engineering Snow, Christopher; Colorado State University, Chemical and Biological Engineering

Porous protein crystals as scaffolds for enzyme immobilization

Ann E. Kowalski,^a Lucas B. Johnson,^a Holly K. Dierl,^a Sehoon Park,^a Thaddaus R. Huber,^a and Christopher D. Snow^a

Received 00th January 20xx,
Accepted 00th January 20xx

DOI: 10.1039/x0xx00000x

www.rsc.org/

Porous protein crystals provide a template for binding and organizing guest macromolecules. Peroxidase, oxidase, and reductase enzymes immobilized in protein crystals retained activity in single-crystal and bulk assay formats. Several binding strategies, including metal affinity and physical entrapment, were employed to encourage enzyme adsorption into the protein crystals and to retain the enzymes for multiple recycles. Immobilized enzymes had lower activity compared to free enzyme in solution, in part due to diffusion limitations of substrate within the crystal pores. However, the immobilized enzymes were long-term stable and showed increased thermal tolerance. The potential applications of enzyme-laden crystals as sensing devices, delivery capsules, and microreactors motivate future development of this technology.

Introduction

Structured biological systems have evolved to provide a variety of benefits in living cells. Designed or natural proteinaceous compartments can be used to balance metabolic flux, prevent off pathway reactions, or sequester toxic intermediates.^{1,2} Creating structured scaffolds *in vitro* can yield similar benefits. Enhancements such as substrate channeling,³ protection from protease degradation,⁴ and coenzyme recycling⁵ make scaffolds particularly appealing for immobilizing enzymatic pathways.

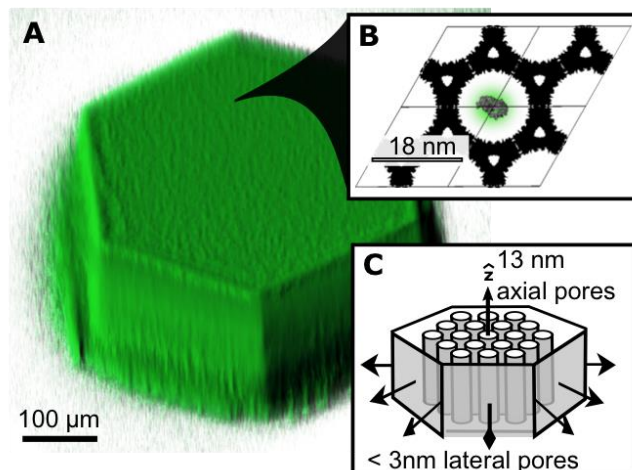
Biological scaffolds created from nucleic acids,⁶ viruses and protein cages,⁷ or other supramolecular assemblies⁸ can position macromolecules with nanometer scale precision and have myriad applications in imaging, sensing, and drug delivery.^{9–11} Furthermore, larger 3-dimensional matrices such as DNA crystals have been shown to function as molecular sieves¹² or enzyme-laden microreactors for biocatalysis.¹³

Porous protein crystals offer an alternative immobilization matrix that can be engineered to display many functional moieties for a wide range of guest attachment strategies.¹⁴

Crystals can grow to hundreds of micrometers in diameter and still be characterized with atomic precision using x-ray diffraction. Much like DNA crystals,¹⁵ porous protein crystals can also be crosslinked to form a robust template and modified to bind guest molecules.^{16,17} Notably, crosslinked protein crystals mimic the crosslinked protein coats used to protect biological spores.¹⁸ Sufficiently large protein crystal solvent pores are suitable for loading larger guests like enzymes.¹⁹

Our previous work with a putative periplasmic polyisoprenoid-binding protein from *Campylobacter jejuni* (CJ) identified a hierarchical pore network that could load and selectively bind fluorescent proteins,²⁰ gold nanoparticles,²¹ and other small molecules, the structure of which could be determined by x-ray diffraction under certain conditions.²² When crystallized in high salt concentrations, CJ grew ~200–600 μm diameter crystals in 1–3 days. The crystals were highly porous with large (13 nm) axial pores and small (~3 nm) perpendicular pores arranged via the P622 space group (Fig. 1). Crosslinking in the presence of a dialdehyde and reducing agent stabilized the crystalline matrix and prevented crystals from dissolving when transferred to water or other low-salt solutions, as well as elevated temperatures, high and low pH solutions, and organic solvents.

In this work we show that several different enzymes can be immobilized within the pores of a crosslinked CJ crystal either by metal affinity or physical entrapment. We demonstrate that two enzymes co-immobilized within the crystal complete a cascade reaction, can be recycled for several uses, and retain activity after long-term storage within the crystal.



^a Department of Chemical and Biological Engineering, Colorado State University, Fort Collins, CO 80521, USA

Electronic Supplementary Information (ESI) available: Supporting figures. See DOI: 10.1039/x0xx00000x

Figure 1. Features of the porous protein crystal CJ. (A) CJ crystal loaded with fluorescently tagged enzyme. (B) Representation of four unit cells from a CJ crystal (Protein Data Bank code 2FGS) with a single peroxidase molecule (green) modelled in the axial nanopore. (C) Schematic of crystal pores and axes.

Experimental

Materials and methods

Protein expression and purification. Horseradish peroxidase (HRP, Pierce™ #31490), HisProbe™-HRP conjugate (hHRP, Pierce™ #15165) and glucose oxidase from *Aspergillus niger* (GOX, SigmaAldrich #G7141) were purchased from commercial suppliers and used without further purification. The codon optimized gene encoding the *Campylobacter jejuni* protein (CJ, GenBank ID CJ0420) was independently cloned into the pSB3 expression vector. CJ was expressed in *E. coli* strains C41(DE3) and BL21(DE3). The target protein was purified from cell lysate via immobilized metal affinity chromatography. Prior to crystallization, CJ was dialyzed into 10 mM HEPES pH 7.5, 150 mM NaCl, 10% glycerol.

Enzymes were fluorescently labeled using blue (CF™405S succinimidyl ester, Biotium #92110), green (NHS-fluorescein, ThermoFisher #46410), or red (CF™594 SE, Biotium #92132) dyes for imaging via confocal fluorescence microscopy.

Protein crystallization and crosslinking. CJ was crystallized via sitting drop vapor diffusion by mixing 1 µl of ~15 mg/mL purified protein with 1 µl of crystallization buffer (3.2-3.5 M ammonium sulfate, pH 6.5). After overnight growth, CJ crystals were crosslinked using glyoxal to improve crystal stability. Glyoxal crosslinking steps consisted of a 30 minute wash in 4.2 M trimethylamine oxide (TMAO) buffer at pH 7.5, a two hour crosslink at room temperature in TMAO supplemented with 1% glyoxal, and a one hour quench in 1 M hydroxylamine with 100 mM DMAB at pH 5.0. These times were optimized previously to ensure complete crosslinking.²⁰ Structures determined via x-ray diffraction have shown that the atomic structure of the crystal remains intact before and after washing and crosslinking,²² and high occupancy of crosslinkers can be achieved.²¹

Confocal microscopy. CJ crystals were attached via UV-curable glue to a glass slide to permit rapid substrate introduction or solution changes. For attachment, a small drop of Bondic™ glue was placed on a clean glass slide. The drop of glue was spread thin using a piece of wire and pre-cured for 5-10 seconds under 365 nm light to a tacky consistency. Next, 10-20 µl of storage buffer (Buffer A) was placed over the drop of glue. A crystal was looped into the solution and pressed gently into the glue with the desired orientation. The glue was cured using a 405 nm LED for another 1-2 mins. Images were collected on a Nikon Eclipse Ti spinning-disk confocal

microscope with an Andor iXon Ultra 897U EMCCD camera. Blue, green, and red fluorescent dyes were imaged using 405 nm, 488 nm, or 561 nm wavelength excitation, respectively. Laser intensity was set to 20% for enzyme detection or 10% for product detection. All images were collected with a 100 ms exposure time and four-frame image averaging.

Activity assays via confocal microscopy. Prior to soaking in enzymes, each crosslinked CJ crystal was incubated for ~1 hr in Buffer A (50 mM HEPES, 300 mM NaCl, 10% glycerol, pH 7.5) with 10 mM nickel sulfate added for metal binding proteins. Crystals were then looped into ~1 mg/mL enzyme solutions in Buffer A and allowed to equilibrate at room temperature for at least one hour.

The activity of the HRP/GOx pathway was assessed on the substrate AmplexRed (ThermoFisher #A12222) by tracking resorufin product fluorescence at 561 nm wavelength excitation. For each reaction, a single enzyme-laden crystal was incubated with 10 µM AmplexRed and 100 µM glucose. Product formation was determined by measuring fluorescence intensity within a 25 µm x 25 µm square in the center of each crystal, or as an average over the entire image. The reaction was performed with three different crystals for each control.

HisProbe-HRP loading via fluorescence plate reader. A minimum of three crystals of known volume were placed in a 150 µL drop of known concentration hHRP in Buffer A (~30 µg/mL). At 0, 20, 40, 60, 80, and 100 minutes, and 20 and 24 hours, a 75 µL sample of the fluorescein-tagged hHRP solution was placed in a Costar black-walled 96-well plate (Corning, CLS3595) and fluorescence intensity was measured via 490 nm wavelength excitation on a FLUOstar Omega plate reader (BMG Labtech). After each measurement, the 75 µL sample was returned to its well and pipetted to mix with the crystals and remaining solution. The fluorescence intensity was compared to a standard curve to determine protein concentration in the well. The standard curve was created using tagged hHRP of known concentrations (Fig. S1).

HisProbe-HRP activity assays via plate reader. Resorufin product formation was monitored at 561 nm wavelength excitation on a FLUOstar Omega fluorescence plate reader (BMG Labtech). 100 µL aliquots of either free hHRP in Buffer A or hHRP immobilized within CJ crystals were used for all experiments. Data was collected every 4-5 seconds after substrate addition, and the 96-well plate was shaken for 1 second between each timepoint.

Results and discussion

Macromolecular guest diffusion

To assess the diffusion of enzyme into the axial pore network, HisProbe horseradish peroxidase (hHRP) was tagged with NHS-fluorescein and soaked into the crystal (Fig. 2). Sodium chloride and glycerol were added to the buffer solution to reduce non-specific

electrostatic and hydrophobic interactions between the guest molecule and the protein scaffold.

Prior to loading hHRP, the crosslinked crystal was soaked in 10 mM NiSO₂ for at least 1 hr. The presence of 6xHisTags on the protein crystal and the tridentate chelator on the hHRP enzyme allowed for coupling of the guest within the pores via shared divalent metal affinity.^{20,21}

A timelapse collected on a confocal microscope showed that hHRP adsorbed strongly into a 100 μm thick crystal over 16 hrs. The crystal was immobilized to a glass slide with UV-curable glue to prevent crystal movement during loading (Fig. 2E). Crystals were typically glued on their lateral side so that the 13 nm axial pores were exposed to solution at both ends of the crystal.

A fluorescence plate reader was used to quantify hHRP loading into CJ crystals over time (Figs. 3, S3). Three or more crystals were placed in a 150 μL well of ~10 μg/mL hHRP in Buffer A. Aliquots of 75 μL of the enzyme solution were sampled at various time points to monitor the decrease in enzyme concentration in the solution as enzyme was adsorbed by the crystals.

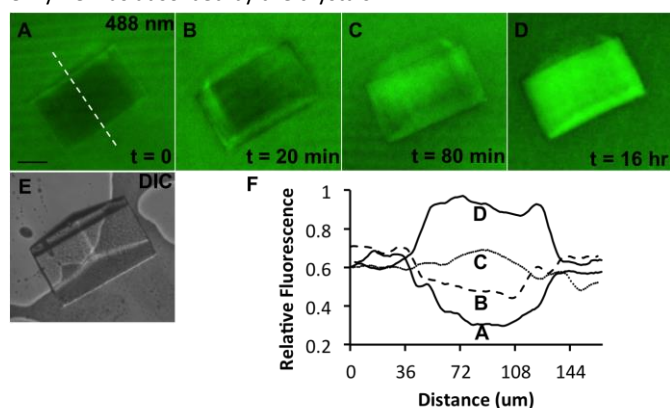


Figure 2. NHS-fluorescein tagged HisProbe horseradish peroxidase (hHRP) at 85 μg/mL diffuses into the pores of a CJ crystal, previously loaded with 10 mM NiSO₄. (A-D) Timelapse images through the center of the crystal on a confocal microscope with 488 nm wavelength excitation. (E) DIC microscopy image showing the CJ crystal glued to a glass slide. (F) Relative fluorescence intensity across the crystal over time as measured by the white dotted line in A. Fluorescence intensity measurements were calculated using ImageJ. Scale bar is 50 μm.

After sampling, the 75 μL aliquot was returned to the well. Crystal volumes were measured using Motic Imaging software to calculate the adsorbed enzyme concentration for each crystal.

Although the equilibrium enzyme concentration inside the crystal is expected to be similar for any size CJ crystal, the rate of loading depends on the crystal surface area, thickness, and volume. Sample 2, which contained the largest total crystal volume, loaded guest enzymes more slowly per unit volume than the other two samples but had a similar equilibrium hHRP loading concentration. The aspect ratio and size of CJ crystals can be tuned by adjusting crystal growth conditions such as pH and salt concentration,²³ providing a potential opportunity to create custom scaffolds with varying loading (or unloading) rates.

Equilibrium conditions were achieved after 24 hours, and enzymes were loaded to a final concentration of ~0.7 mM inside the crystals.

The original enzyme concentration in solution was approximately 0.23 μM; thus, the enzyme adsorbed well beyond the concentration expected by pure diffusion. If one hHRP could bind to every HisTag presented in the crystal pores, the loading concentration would be expected to reach approximately 14 mM. Close packing within the crystal pores prevents every HisTag from being able to bind with large guest molecules. Instead, the apparent loading is 7 hHRP for every 10 unit cells.

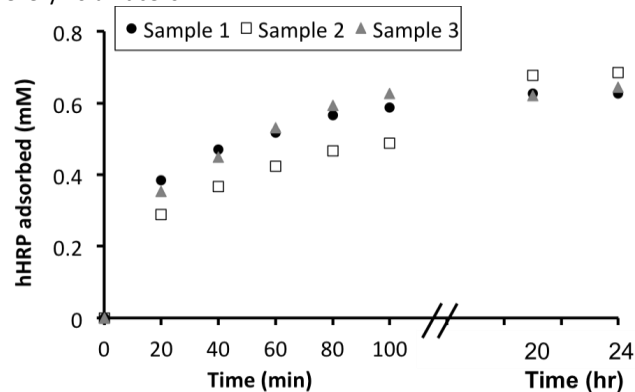


Figure 3. Quantification of HisProbe horseradish peroxidase (hHRP) loading using a fluorescence plate reader with 485 nm wavelength excitation. The concentration of hHRP adsorbed into a crystal of known volume is calculated for three samples over time.

The strong adsorption of hHRP contrasts with the passive loading of proteins that lack metal affinity, such as bovine serum albumin (BSA) (Fig. S4). BSA diffused through the axial pore network of a ~80 μm thick crystal in 20-30 minutes. The fluorescence inside the crystal approached the fluorescence of the surrounding bulk solution over time.

Immobilized enzyme activity

After assessing single enzyme loading and retention within CJ crystals, we demonstrated that it was possible to simultaneously load a second guest, glucose oxidase (GOx), and that both enzymes were catalytically active within the crystal pores (Fig. 4). In the two-step GOx/hHRP pathway, GOx reacted with D-glucose and oxygen to form D-gluconolactone and hydrogen peroxide. hHRP reacted with AmplexRed and hydrogen peroxide to form resorufin and oxygen. Both enzymes (hHRP and GOx), as well as both substrates (glucose and AmplexRed) needed to be present for the resorufin product to be formed.

Crystals were again immobilized to a glass slide with UV-curable glue. The same enzyme pathway was tested on a crystal in free solution to confirm that the presence of the glue did not alter the reaction (Fig. S5). Crystals were first loaded with hHRP by soaking for a minimum of one hour in Buffer A plus 10 mM nickel sulfate and then soaking for at least one hour in 0.5 mg/mL hHRP in Buffer A. The crystal was subsequently loaded with 1.5 mg/mL glucose oxidase (GOx) for 2 hours. The GOx, lacking a metal-chelating group, was physically trapped within the crystal pores by briefly exposing loaded crystals to a solution of 1% glyoxal and 1 mg/mL BSA. Although this entrapment method did not ensure precise

placement of GOx within the pores, as metal affinity does, it provided additional benefits for intermediate channeling as discussed later.

To observe product formation from the GOX/hHRP pathway, the storage solution (Buffer A) was removed and 20 μL of substrate solution (Buffer A supplemented with 10 μM AmplexRed and 100 μM glucose) was pipetted onto the crystal on the glass slide. Confocal excitation at 561 nm wavelength distinctly showed fluorescent product formation throughout the crystal when both enzymes and substrates were present. In less than 30 seconds, resorufin began diffusing into the surrounding bulk solution.

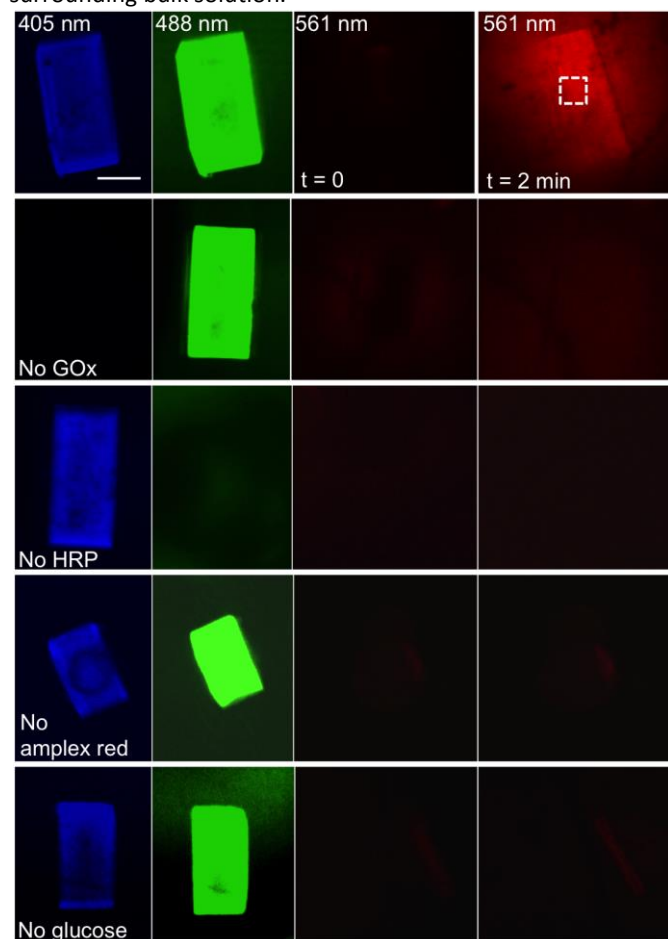


Figure 4. Spinning disk confocal microscope imaging of the GOx/hHRP enzyme pathway inside host crystals. Scale bar is 100 μm . A CJ crystal was loaded with 1.5 mg/mL glucose oxidase (GOx) and 0.5 mg/mL HisProbeTM horseradish peroxidase (hHRP) (top row), only hHRP (second row), or only GOx (third row). The crystal was exposed to 100 μM glucose and 10 μM AmplexRed (top three rows), only glucose (fourth row), or only AmplexRed (bottom row). GOx, tagged with CFTM405S, fluoresces blue under 405 nm wavelength excitation (left column). hHRP, tagged with fluorescein, fluoresces green under 488 nm wavelength excitation (second column from left). The formation of resorufin required both enzymes and both substrates. Resorufin fluoresces red under 561 nm wavelength excitation (right two columns).

Figure 5 shows the increasing pixel intensity as resorufin product was formed in assays with three different crystals. Pixel intensity was corrected for crystal volume, as a larger crystal volume resulted in a larger number of active enzymes and thus a higher overall pixel intensity. Negative controls confirmed that product formation only occurred in the presence of a complete GOx/hHRP pathway. In the absence of GOx, HRP, AmplexRed, or glucose, minimal to no resorufin production was observed. Over two minutes, the average pixel intensity of crystals loaded with both enzymes was greater than 100 times higher than that of any negative control.

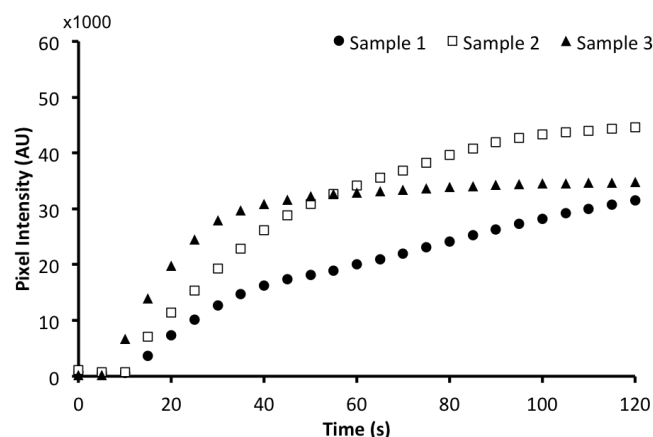


Figure 5. Pixel intensity under 561 nm wavelength excitation, as measured by averaging a 25x25 μm box within each crystal (demonstrated in the top row of Fig. 4), increases in the presence of both enzymes and substrates for three samples. The negative controls have almost negligible pixel intensity. Average pixel intensity was calculated using ImageJ.

Immobilized enzymes often exhibit reduced activity compared to their free counterparts, as a result of transport limitations, or the loss or inhibition of active enzymes.¹³ Due to the relatively gentle immobilization strategy used to adsorb hHRP to the host crystals, we hypothesized that transport limitations could play a dominant role in reducing activity. To test this hypothesis, hHRP was entrapped within several CJ crystals of varying size (Figs. 6, S6).

Figure 6 shows resorufin formation over time from the same concentration of free hHRP in solution and hHRP immobilized within two crystal samples. The “Immobilized Enzyme 1” sample consisted of one crystal of known dimensions (94 μm height, 214 μm diameter). The “Immobilized Enzyme 2” sample consisted of two crystals of approximately the same total volume (5.6 nanoliters). Therefore, when both samples are fully equilibrated with hHRP, both samples should contain about the same total amount of enzyme (0.38 mM or 0.09 \pm 0.0019 μg , as calculated from Fig. 3 and the known crystal volumes). Despite containing the same quantity of enzyme, the rate of product formation for the two immobilized enzyme samples was markedly different. The sample with two smaller crystals, despite containing about the same amount of enzyme as the sample with one larger crystal, had a 16.2% larger surface area and thus a larger surface-to-volume ratio (Fig. S7, Table S1). More hHRP enzyme was

accessible to the substrate during the reaction, which increased the rate of product formation for the two crystal samples. Immobilized enzyme samples were exposed to the same substrate concentrations, 100 μM AmplexRed and 100 μM H_2O_2 , and both had lower rates of product formation than the same concentration of free enzyme in solution.

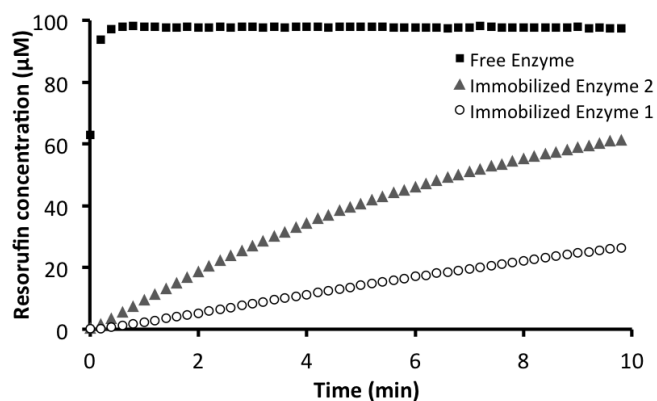


Figure 6. Diffusion limitations within the protein crystal pores alter the activity of the immobilized enzyme. Each sample consisted of 0.38 mM hHRP either free in 100 μL of Buffer A or immobilized via Ni(II) affinity within a crystal sample, incubated in 100 μL of Buffer A. The height and volume of Immobilized Enzyme 1 and 2 were similar, but the surface area of Immobilized Enzyme 2 was 16.2% larger. Each sample was reacted with 100 μM AmplexRed and 100 μM H_2O_2 .

To determine the kinetic parameters for immobilized hHRP, the enzyme was immobilized within micrometer and sub-micrometer diameter crystals. Quijoch and Richards proposed in 1966 that most enzyme crystal transport limitations could be removed by using enzyme crystals less than 5 microns across.²³ Compared to the larger CJ crystals (e.g. hundreds of microns across) typically used for imaging, the diffusion path length from the bulk solution to the center of the microcrystal was much shorter, and therefore a larger fraction of immobilized enzyme was readily accessible to the substrate. Kinetic differences here between free and microcrystal-immobilized enzyme could instead be attributed to steric hindrance or active site inhibition of the immobilized enzyme. Michaelis-Menten kinetic parameters K_{cat} and K_{m} were determined for 0.1 nM hHRP samples in Buffer A and immobilized in microcrystals at substrate concentrations ranging from 0.1 - 100 μM (Table 1, Fig. S9-S12).

Table 1. Average and standard deviation of Michaelis-Menten kinetic parameters for samples of free hHRP in Buffer A and Ni(II)-immobilized hHRP within microcrystals. Data was collected from triplicate samples (see Supporting Information).

	K_{m} (μM)	K_{cat} (1/s)
Microcrystal-immobilized enzyme	48.5 ± 7	245 ± 30
Free enzyme	62.3 ± 7	784 ± 67

Immobilized enzyme stability

Recycle or reuse is one benefit of enzyme immobilization. To test a CJ crystal's capacity for long-term enzyme entrapment and retention of enzyme activity within the crystal, sample 3 from Figure 4 was reused in multiple cycles (Fig. 7). After the initial experiment, the crystal was washed in a large volume of Buffer A for 48 hours to allow residual resorufin product to fully release from the crystal pores. To ensure stable imaging during confocal imaging, the crystal was then immobilized using UV-curable glue and exposed to 10 μM AmplexRed and 100 μM glucose (cycle 2). After cycles 2 and 3, the crystal was removed from the UV-glue, washed for 30 minutes to remove residual resorufin, and then re-glued to a glass slide. After cycle 4, the crystal was incubated in a large reservoir of Buffer A at room temperature for 16 days prior to use in cycle 5. It is remarkable and promising that enzyme-crystal activity was maintained after multiple handling steps, washing, and gluing.

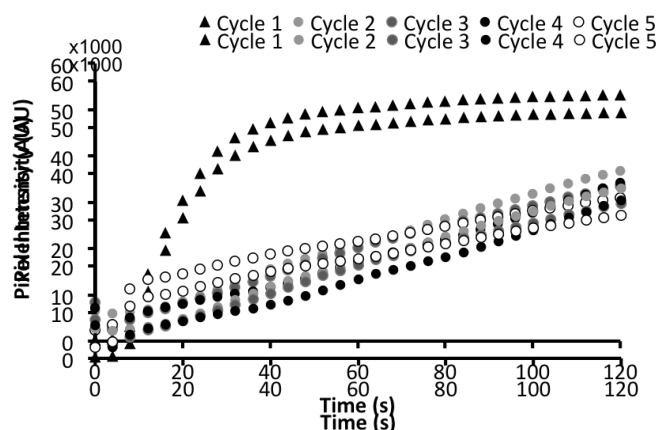


Figure 7. Crystal sample 3 from Figure 5, after the initial experiment (cycle 1), was washed for 48 hrs in large reservoir of Buffer A prior to use in cycles 2 through 4. The crystal was washed in Buffer A for 30 minutes between each cycle 2 through 4 to remove residual resorufin. The crystal was then incubated in a large reservoir of Buffer A for 16 days prior to cycle 5. Cycles 2 through 5 consisted of exposure to 100 μM glucose and 10 μM AmplexRed, as in Figure 4. Fluorescence intensity was detected under 561 nm wavelength excitation on a spinning disk confocal microscope.

We hypothesize that the initial loss of fluorescence between cycle 1 and cycle 2 could be caused by loss of GOx enzyme due to incomplete BSA/glyoxal crosslinking. It is likely that some unbound enzyme diffused from the crystal pores during the 48 hour wash period. When a similar experiment was performed using BSA and glutaraldehyde (Fig. S13), activity was maintained at a more consistent rate after multiple use cycles. Glutaraldehyde is highly reactive and readily polymerizes,^{25,26} likely resulting in higher enzyme retention within the crystal. Even after three days storage in Buffer A at 4°C and five reuse cycles, the GOx/BSA/glutaraldehyde crystal maintained >85% relative activity. A crystal stored at 4°C for 62 days displayed low but detectable activity on AmplexRed.

Additional potential benefits of entrapping enzymes within a porous scaffold may be the selective exclusion of otherwise disruptive molecules and the channeling of reaction intermediates. For example, in the coupled GOx/hHRP enzyme reaction, H_2O_2 is an intermediate. Therefore, an enzyme that reacts with H_2O_2 , such as catalase, can reduce the formation of resorufin. Since catalase is fairly large, we sought to exclude it from the CJ crystal nanopores by forming a physical barrier at the crystal surface. Specifically, we applied BSA and glutaraldehyde crosslinking to form a shell around the CJ crystals. This strategy was partially successful in that a crystal with a BSA/glutaraldehyde shell had lower catalase loading than a similar crystal without a shell (Fig. S14), and the GOx/HRP pathway within a shell-protected crystal proceeded at the same rate whether catalase was present in solution or not (Fig. S15). In the future, the defined nanoporous structure could afford other opportunities to rationally gate the transport of macromolecules into and out of the crystal based on size exclusion principles.

Enhanced thermal tolerance is often a benefit of enzyme immobilization.²⁷ In order to test the thermal stability of hHRP enzyme immobilized within CJ crystals, a known quantity of hHRP was loaded into two equally-sized crystals. Resorufin production from both samples was monitored using a fluorescence plate reader (Fig. 8). One sample was kept at room temperature while the second sample was incubated at 45°C for 10 minutes prior to the reaction. The second sample was also maintained at 45°C throughout the reaction. The experiment was simultaneously performed on the same concentration of free enzyme in solution. Free enzyme in solution at 45°C exhibited decreased rates of product formation and lower overall product formation than free enzyme at room temperature. In contrast, enzymes within CJ crystals were more active at 45°C, which we attribute to some combination of enhanced substrate and product diffusion and host-crystal conferred heat tolerance. More surprising still was the observation that high temperature (e.g. 80°C) pre-incubation of hHRP loaded crystals decreased activity significantly less than 80°C pre-incubation of free enzyme (Figs. S16, S17).

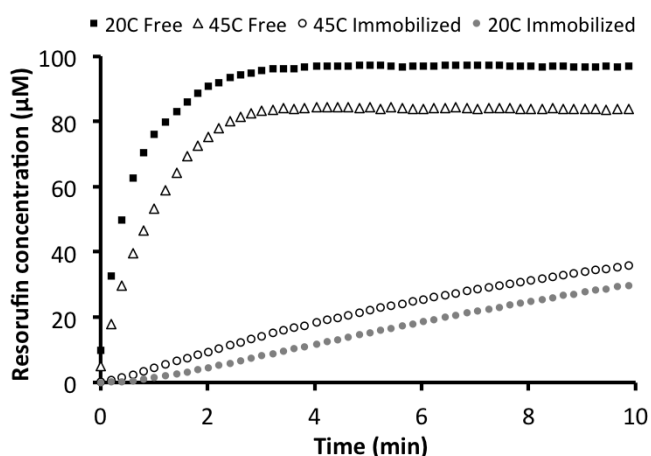


Figure 8. At 45°C, free enzyme in solution (45C free) had lower rates of product formation than free enzyme at room temperature (20C

Free). Immobilized hHRP incubated at elevated temperature had a higher rate of product formation than the same concentration of immobilized enzyme at room temperature. All reactions were performed with 100 μ M AmplexRed and 100 μ M H_2O_2 . Resorufin production was monitored under 561 nm wavelength excitation using a fluorescence plate reader.

To confirm that this immobilization strategy was generalizable to other target enzymes, xylose reductase (XR) and glycerol dehydrogenase (GDH) were co-immobilized within a CJ protein crystal (Fig. S18). XR and GDH were both engineered to display HisTags, which can bind Ni^{+2} similarly to the HisProbeTM chelator.^{20,21} Xylitol production, through the reduction of xylose by XR, was monitored using high-performance liquid chromatography (HPLC) (Fig. S19). However, preliminary experiments with GDH suggested insufficient product formation to be assessed with HPLC. Unlike previous experiments, product formation was detected through a bulk assay of five crystals after a 30 minute reaction time.

Conclusions

The benefits of crosslinked protein crystals²⁷ and crosslinked enzyme crystals²⁸ have been reported for many years. However, these benefits have only been accessible in the past if researchers were willing to optimize crystal growth conditions for their enzyme of interest. Engineered highly porous protein crystals with connected solvent channels provide new opportunities for enzyme immobilization. Host protein crystals can be loaded with diverse enzymes or enzyme mixtures, greatly expanding the list of potential applications.

We show here that porous protein crystals can be used to synthesize novel host-guest catalytic materials via controlled loading of macromolecules. Enzymes can be immobilized within the crystal pores, and a two-enzyme pathway remained active for several recycles over multiple weeks. The preliminary favourable thermo-stabilization effects observed here for guest enzymes suggest that it may be possible to confer some of the remarkable thermotolerance or solvent-tolerance properties of crosslinked enzyme crystals onto guest enzymes installed within porous host crystals.

Other protein crystals with smaller or larger pore sizes could be used to tailor specific diffusion properties. The range of possible protein modifications and crystal sizes provides a versatile and robust crystalline chassis for enzyme immobilization.

Conflicts of interest

There are no conflicts to declare.

Acknowledgements

This material is based in part upon work supported by the National Science Foundation under Grant Numbers 1434786 and 1506219.

Notes and references

1. Chen, A. H. & Silver, P. A. *Trends Cell Biol.* 2012, **22**, 662–670.
2. Conrado, R. J., Varner, J. D. & DeLisa, M. P.. *Curr. Opin. Biotechnol.* 2008, **19**, 492–499.
3. Fu, J., Liu, M., Liu, Y., Woodbury, N. W. & Yan, H. *J. Am. Chem. Soc.* 2012, **134**, 5516–5517.
4. Zhao, Z. *et al. Nat. Commun.* 2016, **7**.
5. Fu, J. *et al. Nat. Nanotechnol.* 2014, **9**, 531–536.
6. Fu, J., Liu, M., Liu, Y. & Yan, H. *Acc. Chem. Res.* 2012, **45**, 1215–1226.
7. de la Escosura, A., Nolte, R. J. & Cornelissen, J. J. *J. Mater. Chem.* 2009, **19**, 2274–2278.
8. Song, W. J. & Tezcan, F. A. *Science* 2014, **346**, 1525–1528.
9. Vriezema, D. M. *et al. Chem. Rev.* 2005, **105**, 1445–1490.
10. Wang, F., Lu, C.-H. & Willner, I. *Chem. Rev.* 2014, **114**, 2881–2941.
11. Lu, C.-H., Willner, B. & Willner, I. *ACS Nano* 2013, **7**, 8320–8332.
12. Paukstelis, P. J. *J. Am. Chem. Soc.* 2006, **128**, 6794–6795.
13. Geng, C. & Paukstelis, P. J. *J. Am. Chem. Soc.* 2014, **136**, 7817–7820.
14. Abe, S., Maity, B. & Ueno, T. *Curr. Opin. Chem. Biol.* 2018, **43**, 68–76.
15. Zhang, D. & Paukstelis, P. J. *ChemBioChem.* 2016.
16. Abe, S. & Ueno, T. *RSC Adv.* 2015, **5**, 21366–21375.
17. Ueno, T. *Chem. Eur. J.* 2013, **19**, 9096–9102.
18. McKenney, P. T., Driks, A. & Eichenberger, P. *Nat. Rev. Microbiol.* 2013, **11**, 33–44.
19. Abe, S., Maity, B. & Ueno, T. *Chem. Commun.* 2016, **52**, 6496–6512.
20. Huber, T. R. *et al. Small.* 2017.
21. Kowalski, A. E. *et al. Nanoscale* 2016, **8**, 12693–12696.
22. Huber, T. (Colorado State University, 2017).
23. Huber, T., McPherson, E., Keating, C., and Snow, C. *Bioconjugate Chem.* 2018, **29**, 17–22
24. Quijcho, F. A. and Richards, F. M. *Biochemistry.* 1966, **5**, 4062–4076
25. Migneault, I., Dartiguenave, C., Bertrand, M. J. & Waldron, K. C. *BioTechniques* 2014, **37**, 790–796, 798–802.
26. Habeeb, A. F. S. A. & Hiramoto, R. *Arch. Biochem. Biophys.* 1968, **126**, 16–26.
27. Margolin, A. L. & Navia, M. A. *Angew. Chem. Int. Ed.* 2001, **40**, 2204–2222.
28. Nancy L. St. Clair, *J. Am. Chem. Soc.* 1992, **114**, 7314–7316.

